Proceedings of the
Annual Stability Conference
Structural Stability Research Council
Louisville, Kentucky, April 13-16, 2021

Expanded benchmark studies on the AISC direct analysis method

Mark D. Denavit[1]

Abstract
Second-order elastic design methodologies such as the direct analysis method established within the AISC *Specification for Structural Steel Buildings* rely, among other things, on broad parametric studies to establish their validity. It is warranted to revisit these studies when modifications to the design methodology are proposed or increases in computational capabilities allow the analysis of a significantly wider parametric set. This work builds off of the original verification studies for the direct analysis method, utilizing second-order inelastic analysis results as a benchmark against which the accuracy of the design methodology is assessed, and expands in two ways. First, wider ranges of cross section parameters are examined, explicitly verifying the direct analysis method for a variety of common steel yield strengths, cross sections, and cross section types (e.g., wide flange and hollow structural section). Second, the validation is extended to variations of the direct analysis method, including the advanced tier of the direct analysis method where member imperfections are included in the analysis and available compression strength is taken as that of the cross section. These expanded validation studies quantify the level of error associated with the design methodologies, identify areas where further investigation is necessary, and provide valuable data for the further development of design standards.

1. Introduction

The AISC *Specification for Structural Steel Buildings* (AISC 2016) permits any method of stability design that considers a list of important physical phenomenon. The *Specification* also describes several specific methods that meet the requirements. The primary methods of design utilize second-order elastic analysis for the determination of required strengths. In these methods, inelasticity (one of the important physical phenomenon that must be considered) is captured through the use of reduced elastic stiffness and in the calculation of available strength. Both must be calibrated to achieve accurate results.

Through comparisons to second-order inelastic analyses, Kanchanalai (1977) calibrated the interaction strength equation for use within the effective length method and Surovek-Maleck and White (2004) calibrated the stiffness reduction for use within the direct analysis method. Both conducted analyses on a variety of frame configurations, but focused on a single wide flange cross section. Wang and Ziemian (2019) evaluated several design methodologies including the

[1] Assistant Professor, University of Tennessee, Knoxville, <mdenavit@utk.edu>

design by advanced elastic analysis method presented in Appendix 1 of the AISC *Specification*. They investigated a variety of cross sections, but focused on one frame configuration. While no parametric study could completely cover the vast range of cases for which the AISC *Specification* is applicable, expanded studies are possible given modern computing power. Moreover, expanded studies are needed to rigorously evaluate the growing range of stability design methods available to engineers.

This paper presents a broad parametric study undertaken to evaluate second-order elastic analysis based stability design methods. The studies investigate a range of cross section types and geometries, material properties, frame configurations, and design methods but are limited to in-plane behavior of doubly symmetric members. The method of evaluation follows that of previous studies, using second-order inelastic analysis results as a benchmark against which the methods of design are compared. These comparisons identify conservative and unconservative error in the design methods and can quantify the impact of specific provisions. This work will help guide further development of design provisions as well as future investigations on the behavior of structural steel frames.

2. Parametric Suite

As with the original benchmark studies for the direct analysis method (Surovek-Maleck and White 2004), as well as other similar studies (Kanchanalai 1977; Denavit et al. 2016), methods of design will be evaluated through comparison to second-order inelastic analysis. The results of the second-order inelastic analysis serve as the "best guess" of the true behavior and the evaluation quantifies how closely the design method based on elastic analysis matches this benchmark. Specifically, the applied loads that the second-order inelastic analysis shows result in failure are compared to the maximum permitted applied loads according to the design methodology. This comparison is made for many small structures which cover a wide range of relevant parameters.

The parametric suite selected for this study is based upon, but expanded from that used in the original benchmark studies for the direct analysis method. The parametric suite considered by Surovek-Maleck and White (2004) included one wide flange cross section and 23 small non-redundant structural frames, all of which were investigated for major-axis bending and 18 of which were investigated for minor-axis bending. The resulting total number of cases was 41. In this study, a wide variety of cross sections will be investigated with the same 23 small structural frames.

2.1. Selected Cross Sections

The cross section investigated by Surovek-Maleck and White (2004) was a W8×31 with yield strength, F_y = 36 ksi. This same cross section was previously investigated by Kanchanalai (1977). The results from these studies are widely applicable given the normalization applied to other parameters (e.g., member length is defined as ratio of length to radius of gyration), however, not all relevant factors are normalized. In particular, the ratio of plastic section modulus to elastic section modulus, often termed the shape factor, may be an important parameter which is missed by only investigating a single cross section in major-axis and minor-axis bending.

For this study, a suite of wide flange and hollow structural section (HSS) shapes was selected for investigation based largely on the shape factor. Of the 283 wide flange shapes listed in the AISC Shapes Database (Version 15.0), 10 were selected and investigated in both major-axis and minor-axis bending. Key properties of these sections are listed in Table 1 and the shape factor is plotted in Figure 1. Of the 340 square and rectangular HSS shapes listed in the AISC Shapes Database for ASTM A1085, 6 were selected and investigated in major-axis bending only. Key properties of these sections are listed in Table 2 and the shape factor is plotted in Figure 2. Of the 112 round HSS shapes listed in the AISC Shapes Database for ASTM A1085, 3 were selected for investigation. Key properties of these sections are listed in Table 3.

Table 1. Selected wide flange shapes

Index	Shape	d	t_w	b_f	t_f	k	Z_x/S_x	Z_y/S_y	$b_f/2t_f$	h/t_w
---	---	in	In	in	in	in	---	---	---	---
1	W8×31[a]	8.00	0.285	8.00	0.435	0.829	1.11	1.52	9.19	22.3
2	W14×43[b]	13.7	0.305	8.00	0.530	1.12	1.11	1.53	7.54	37.4
3	W14×120	14.5	0.59	14.7	0.94	1.54	1.12	1.51	7.80	19.3
4	W14×311	17.1	1.41	16.2	2.26	2.86	1.19	1.53	3.59	8.09
5	W14×730	22.4	3.07	17.9	4.91	5.51	1.30	1.55	1.82	3.71
6	W18×311	22.3	1.52	12.0	2.74	3.24	1.21	1.57	2.19	10.4
7	W21×62[b]	21.0	0.40	8.24	0.615	1.12	1.13	1.55	6.70	46.9
8	W40×264[b]	40.0	0.96	11.9	1.73	2.91	1.16	1.60	3.45	35.6
9	W40×392	41.6	1.42	12.4	2.52	3.70	1.19	1.63	2.45	24.1
10	W40×593	43.0	1.79	16.7	3.23	4.41	1.18	1.59	2.58	19.1

[a] Flange is noncompact for flexure for F_y = 50 and 65 ksi
[b] Web is nonslender for compression for some or all selected yield strengths

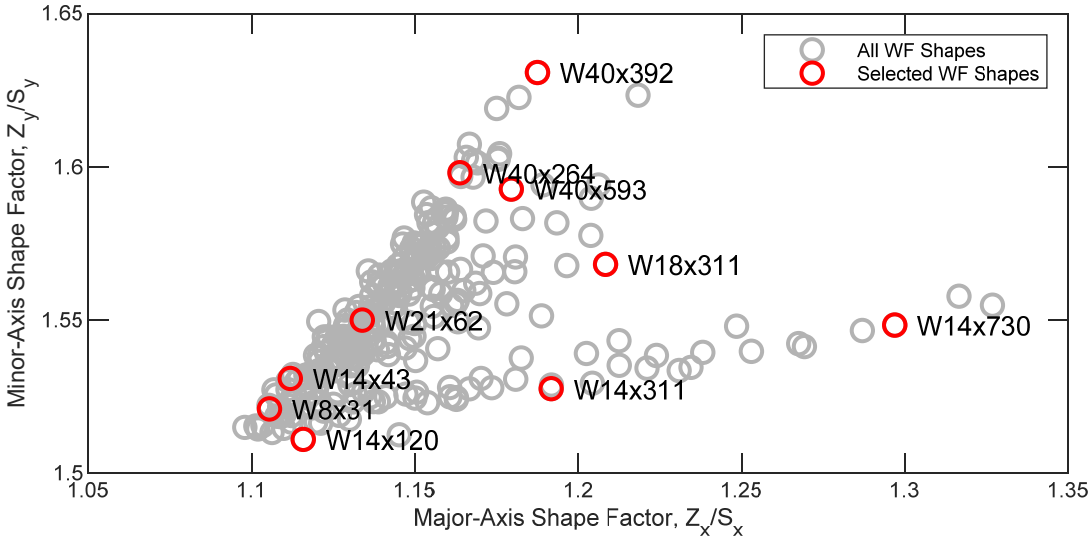

Figure 1. Selected wide flange shapes

Each selected steel shape is analyzed with three different yield strengths, F_y = 36, 50, and 65 ksi. This results in a total of 30 wide flange cross sections, 18 square and rectangular cross sections, and 9 round HSS cross sections investigated. Note that while all the selected shapes are currently produced with F_y = 50 ksi, either as ASTM A992 for the wide flange shapes or ASTM A1085 for

the HSS shapes, the shapes may not be available with F_y = 36 or 65 ksi. These yield strengths were selected to achieve a range, not necessarily to represent specific available members.

The effects of local buckling are not included in the second-order inelastic analysis and design provisions for local buckling were not used (i.e., all sections were treated as compact). As noted in Table 1, Table 2, and Table 3, some of the cross sections are not compact for either flexure or compression at the selected yield strengths. It is anticipated that results of this broad investigation will guide the selection of parameters in future studies using more detailed models (e.g., using shell finite elements) that can capture local buckling.

Table 2. Selected square and rectangular HSS shapes

Index	Shape	H	B	t	Z_x/S_x	h/t	b/t
---	---	in	in	in	---	---	---
1	HSS16×16×3/8[a,b]	16	16	0.375	1.16	39.7	39.7
2	HSS6×6×3/8	6	6	0.375	1.21	13.0	13.0
3	HSS4×4×3/8	4	4	0.375	1.26	7.67	7.67
4	HSS3×3×3/8	3	3	0.375	1.31	5.00	5.00
5	HSS8×4×5/8	8	4	0.625	1.35	9.80	3.40
6	HSS10×2×3/8	10	2	0.375	1.42	23.7	2.33

[a] Flange is noncompact for flexure for all selected steel yield strengths
[b] Walls are slender for compression for F_y = 50 and 65 ksi

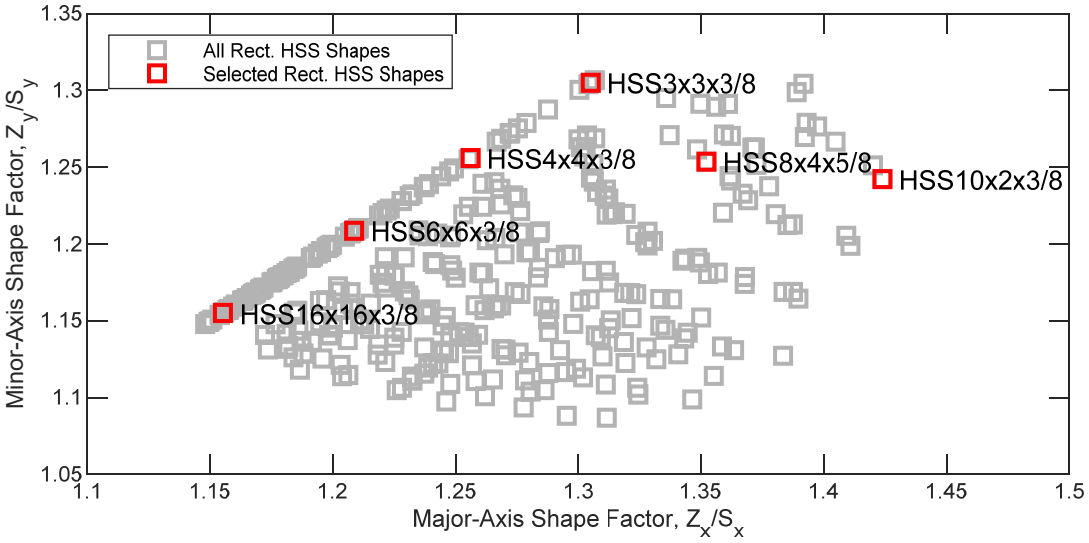

Figure 2. Selected square and rectangular shapes

Table 3. Selected round HSS shapes

Index	Shape	D	t	Z_x/S_x	D/t
---	---	in	in	---	---
1	HSS20.000×0.500[a]	20.0	0.5	1.30	40.0
2	HSS7.500×0.500	7.5	0.5	1.35	15.0
3	HSS5.000×0.500	5.0	0.5	1.41	10.0

[a] Shape is noncompact for flexure for F_y = 65 ksi

2.2. Selected Frames

The 23 frames that were investigated by Surovek-Maleck and White (2004) are investigated in this work. The frames are either sidesway uninhibited or sidesway inhibited as shown in Figure 3. The stiffness of the rotational springs at the top and bottom of the column is defined by the parameter G by Eq. 1. Where $G = 0$, the stiffness of the rotational spring is infinite and the spring is replaced with a boundary condition.

$$k_\theta = \frac{6EI}{GL} \tag{1}$$

The parameters for each of the 23 frames is listed in Table 4. For simplicity, all 23 frames were utilized for each selected cross section, regardless of bending axis.

The members were assumed to have initial geometric imperfections. For the sidesway uninhibited frames, this consisted of an out-of-plumbness of $L/500$ and an out-of-straightness of $L/1000$. For the sidesway inhibited frames, only an out-of-straightness of $L/1000$ was assumed.

Table 4. Selected frames

Index	Designation	Sidesway	L/r	G_{top}	G_{bot}	γ	β
1	UP_S20_G0_α3	Uninhibited	20	0	∞	3	---
2	UP_S20_G1_α3	Uninhibited	20	1	∞	3	---
3	UP_S40_G0_α2	Uninhibited	40	0	∞	2	---
4	UP_S40_G1_α2	Uninhibited	40	1	∞	2	---
5	UR_S40_G0_α2	Uninhibited	40	0	0	2	---
6	UR_S40_G0_α3	Uninhibited	40	0	0	3	---
7	UR_S80_G0_α1	Uninhibited	80	0	0	1	---
8	UR_S80_G0_α2	Uninhibited	80	0	0	2	---
9	UR_S80_G0_α3	Uninhibited	80	0	0	3	---
10	SP_S20_G0	Uninhibited	20	0	∞	0	---
11	SP_S40_G0	Uninhibited	40	0	∞	0	---
12	SP_S40_G3	Uninhibited	40	3	∞	0	---
13	SP_S60_G0	Uninhibited	60	0	∞	0	---
14	SP_S80_G0	Uninhibited	80	0	∞	0	---
15	SP_S80_G3	Uninhibited	80	3	∞	0	---
16	SR_S40_G0	Uninhibited	40	0	0	0	---
17	SR_S40_G3	Uninhibited	40	3	3	0	---
18	SR_S80_G0	Uninhibited	80	0	0	0	---
19	SR_S80_G3	Uninhibited	80	3	3	0	---
20	SCB_S80	Inhibited	80	---	---	---	1.0
21	SCB_S120	Inhibited	120	---	---	---	1.0
22	DCB_S80	Inhibited	80	---	---	---	-0.5
23	DCB_S120	Inhibited	120	---	---	---	-0.5

3. Second-Order Inelastic Analysis

The second-order inelastic analyses were performed in the OpenSees framework using a mixed beam finite element formulation in two dimensions and with fiber cross sections. Six elements were used along the length of the member, each with five integration points. The maximum size of each fiber was taken as $1/30^{th}$ of the height of the cross section. Initial geometric imperfections were modeled directly through definition of node coordinates.

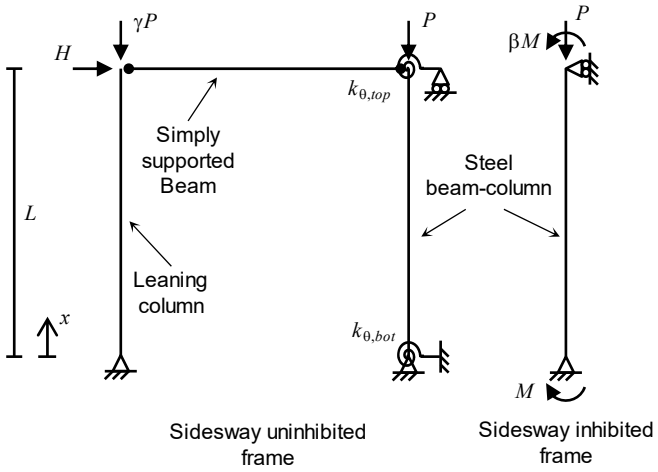

Figure 3. Schematic of benchmark frames

A bilinear stress-strain relationship was used for the wide flange cross sections with hardening modulus equal to $E/1000$. The fillet between the flange and the web was included in the fiber discretization. Residual stresses were defined as an initial stress in the uniaxial stress-strain relationship assigned to each fiber and were assumed to follow the Lehigh residual stress pattern (Galambos and Ketter 1959). However, noting that the Lehigh residual stress pattern may not be representative of the residual stress in the broad range of cross sections selected for investigation and that rotary-straightening processes may significantly reduce residual stresses (Ge and Yura 2019), each analysis was also performed without residual stress.

A multilinear stress-strain relationship based on that described by Abdel-Rahman and Sivakumaran (1997) was used for the HSS cross sections. The material is elastic to a stress of $0.75F_y$ at which point the modulus reduces to $E/2$. The modulus further reduces to $E/10$ at a stress of $0.875F_y$ and finally to a modulus of $E/1000$ at a stress of F_y. Abdel-Rahman and Sivakumaran recommend a modulus of $E/200$ as the final modulus, but a value of $E/1000$ was used to match the assumptions in the model for the wide flange sections. Additionally, the increase in strength in the corner regions of square and rectangular sections recommended by Abdel-Rahman and Sivakumaran was not included. The fiber discretization accounted for the radius of the corners of the square and rectangular HSS. The internal radius of the corners was taken as the thickness of the tube.

Example results from the second-order inelastic analysis are shown in Figure 4a. These results are for a wide flange section (shape index 1, Table 1) with F_y = 50 ksi and bent about the minor-axis. The frame is sidesway uninhibited (farme index 1, Table 4). Interaction diagrams representing applied loads and internal forces for both with and without residual stresses are shown. The axial loads are normalized by the yield load, $P_y = F_y A_g$ which equals 456 kips for this example and the bending moments are normalized by the plastic moment $M_p = F_y Z$ which equals 705 kip-in for this example.

The applied loads interaction diagrams represent the maximum loads which can be applied to the model. For the sidesway uninhibited frames, the applied lateral load, H, is a force. This is converted to a moment for plotting purposes by multiplying by a characteristic length. The frame

examined in Figure 4 is free to rotate at the bottom and fixed against rotation at the top, therefore the characteristic length was set equal to L. The internal forces interaction diagrams represent the maximum internal forces along the length of the member that occur simultaneously with the peak applied loads. The internal moment is greater than the applied moment since it includes the P-Δ and P-δ effects.

The interaction diagrams shown in Figure 4a were constructed from several analyses. First, an analysis was performed applying vertical load only. The vertical load, P (Figure 3), was increased in displacement control until a maximum was identified. The maximum value of P from this analysis is plotted on the y-axis for the applied load interaction (i.e., zero applied lateral load) and with the maximum internal bending moment that occurred simultaneously with the maximum value of P for the internal forces interaction diagrams. Then, a series of non-proportional analyses was performed. For each non-proportional analysis, a vertical load was applied in load control then held constant, then the lateral load, H in this case or M for the sidesway inhibited frames, was increased in displacement control until a maximum was identified. The applied loads and internal forces at the limit point were recorded and plotted. As can be seen in Figure 4a, residual stresses had a deleterious effect on the axial strength, but no effect on the pure moment strength, as the limit state was flexural yielding and the strength was simply equal to the plastic moment.

4. Second-Order Elastic Analysis

The second-order elastic analyses were performed via closed-form solutions obtained using a computer algebra system. The governing differential equation includes the effect of initial geometric imperfections to accommodate direct modeling of both system and member imperfections where necessary. The governing differential equation is given by Eq. 2.

$$v''''(x) + \frac{P}{EI^*}\left[v''(x) + v_o''(x)\right] = 0 \tag{2}$$

where, v is the lateral deflection, P is the axial compression load, EI^* is the flexural stiffness of the beam-column with reductions as appropriate for the design method, and v_o is the initial geometric imperfection given by Eq. 3.

$$v_o(x) = \Delta_o \frac{x}{L} + \delta_o \sin\left(\frac{\pi x}{L}\right) \tag{3}$$

where, Δ_o is the magnitude of the initial out-of-plumbness and δ_o is the magnitude of the initial out-of-straightness.

Boundary conditions for the two frame types and finite rotational spring stiffness are listed in Table 5. Alternative boundary conditions were used when the stiffness of the rotational springs was infinite. For example, the second boundary condition for the sidesway uninhibited frame was taken as $v'(0) = 0$ when $k_{\theta,bot}$ was infinite. The closed-form solutions agreed with the results of OpenSees analyses.

Where an effective length factor, K, was necessary, it was back-calculated from the critical load obtained using the same differential equation and boundary conditions.

Table 5. Benchmark frame boundary conditions

Boundary Condition	Sidesway Uninhibited Frame	Sidesway Inhibited Frame
1	$v(0)=0$	$v(0)=0$
2	$-EI^{*}v''(0)=-k_{\theta,bot}v'(0)$	$-EI^{*}v''(0)=M$
3	Eq. 4	$v(L)=0$
4	$-EI^{*}v''(L)=k_{\theta,top}v'(L)$	$-EI^{*}v''(L)=\beta M$

$$-EI^{*}v'''(L)-P\left[v'(L)+v_o'(L)\right]=H+\frac{\gamma P}{L}\left[v(L)+v_o(L)\right] \tag{4}$$

5. Design Methods

Five separate design methods were investigated in this work as detailed in Table 6. They include: the effective length method as defined in Appendix 7 of the AISC *Specification*, three versions of the direct analysis method as defined in Chapter C, and the design by advanced elastic analysis method as defined in Appendix 1. In each method, the required strengths are computed from a second-order elastic analysis and the available strength is computed using the equations in Chapters E, F, and H of the AISC *Specification*. Note that all comparisons performed in this work are at the nominal strength level, without resistance factors applied.

Table 6. Details of design methods

Index	Description	System Imperfections	Member Imperfections	EI^{*}	L_c
1	Effective Length	Notional Loads[a]	Not Modeled	EI	KL
2	Direct Analysis	Notional Loads	Not Modeled	$0.8\tau_b EI$	L
3	Direct Analysis	Notional Loads[a]	Not Modeled	$0.8\tau_b EI$	L
4	Direct Analysis ($\tau_b = 1$)	Notional Loads[a,b]	Not Modeled	$0.8EI$	L
5	Advanced Elastic Analysis	Direct Modeling	Direct Modeling	$0.8\tau_b EI$	0

[a] Notional load taken as a minimum lateral load when ratio of second-order drift to first-order drift ≤ 1.7

[b] Additional notional load applied in accordance with Section C2.3(c) of the AISC *Specification* (2016)

In the effective length method, the second-order elastic analysis utilizes nominal stiffness values and available strengths are computed using an effective length equal to the unsupported length of the column, L, times the effective length factor, K. As noted previously, the effective length factor used in this work was computed from the governing differential equations. Appendix 7 of the AISC *Specification* limits the use of the effective length method to when the ratio of maximum second-order drift to maximum first-order drift is equal to or less than 1.5. However, this limit was neglected in this work.

Example results from the effective length method are shown in Figure 4b. For the case examined in Figure 4, the effective length factor is K = 3.72. The interaction diagram computed in accordance with Chapter H of the AISC *Specification* with $L_c = KL$ is shown as the internal forces interaction diagram since the maximum internal forces along the length of the member are used within the interaction equation to assess strength. An applied loads interaction diagram is

also shown. This interaction diagram is computed iteratively as the maximum applied loads permitted by the design methodology. In other words, the applied loads that, when applied in a second-order elastic analysis following the requirements of the effective length method result in required strengths that lay on the internal forces interaction diagram (i.e., interaction ratio of 1.0). The grey horizontal line represents the axial load at which the ratio of maximum second-order drift to maximum first-order drift equals 1.5. Above the grey line, a portion of the applied loads interaction diagram is also horizontal. The horizontal portion is at the axial load at which the ratio of maximum second-order drift to maximum first-order drift equals 1.7. Section C2.2b(d) of the AISC *Specification* permits the notional loads that represent the initial system imperfection be taken as a minimum lateral load if the second-order drift ratio is equal to or less than 1.7 in all load combinations. For second-order drift ratios greater than 1.7, the notional loads are additive.

In the direct analysis method, the second-order elastic analysis utilizes reduced stiffness and available strengths are computed with an effective length equal to the unsupported length of the column, L. Example results from the direct analysis method are shown in Figure 4c. Three variations are plotted, corresponding to design methods 2, 3, and 4 as listed in Table 6. The internal forces interaction diagram for all three is the same and equal to that computed in accordance with Chapter H of the AISC *Specification* with $L_c = L$. For design method 2, the notional load is always additive (i.e., the provision in Section C2.2b(d) was not invoked). As a result, there is no portion of the applied load interaction diagram that is horizontal. For design method 3, the provision in Section C2.2b(d) was invoked and the notional loads were taken as minimum lateral loads for second-order drift ratios less than or equal to 1.7. Note that the load at which the second-order drift ratio equals 1.7 differs between Figure 4b and Figure 4c since stiffness reductions apply for the direct analysis method. For design method 4, an additional notional load (that is always additive) was included and the factor τ_b was taken as 1.0 in accordance with Section C2.3(c) of the AISC *Specification*. Implementing the τ_b factor, which depends on axial load, can be cumbersome in practice. For this case, this simplification is conservative (i.e., reduces the maximum permitted applied load), however this may not always be the case.

In the design by advanced elastic analysis method, the second-order elastic analysis utilizes reduced stiffness and system and member imperfections are modeled directly. The previous methods utilized notional loads to represent system imperfections and member imperfections were not modeled. In exchange for the more complicated handling of initial geometric imperfections, the available strength is computed using an effective length of zero. Example results from the design by advanced elastic analysis method are shown in Figure 4d. As can be seen, the internal forces interaction diagram intersects the y-axis at 1.0 indicating that the axial strength is simply equal to the yield load, P_y.

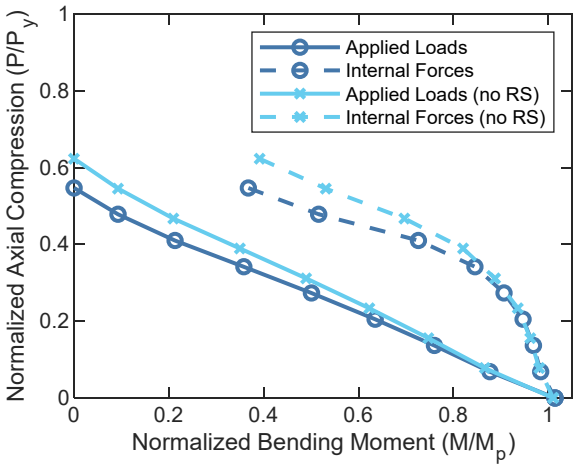

(a) Second-order inelastic analysis results

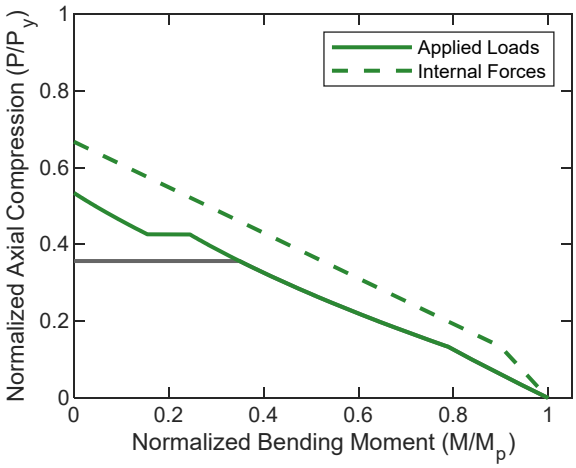

(b) Effective length method results
(Method 1 from Table 6)

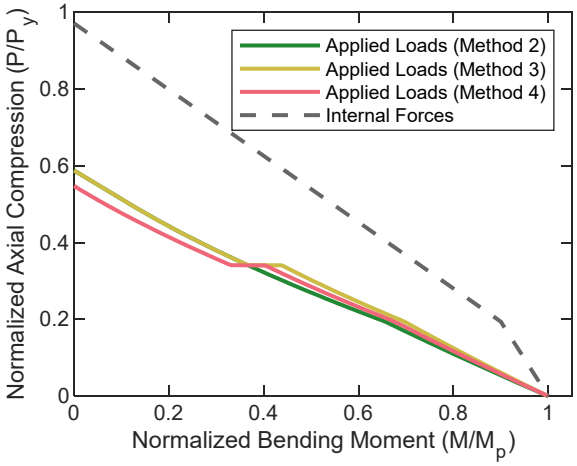

(c) Direct analysis method results
(Methods 2, 3, and 4 from Table 6)

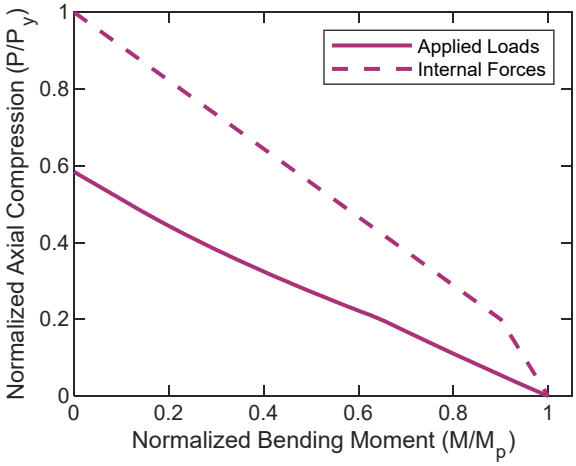

(d) Advanced elastic analysis method results
(Method 5 from Table 6)

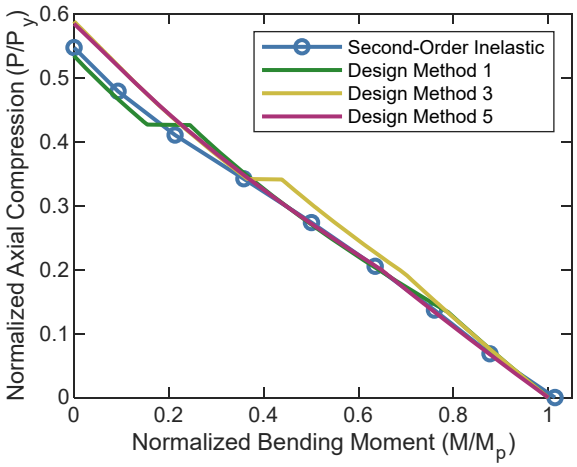

(e) Comparison of applied load curves to second-order inelastic analysis (with residual stress)

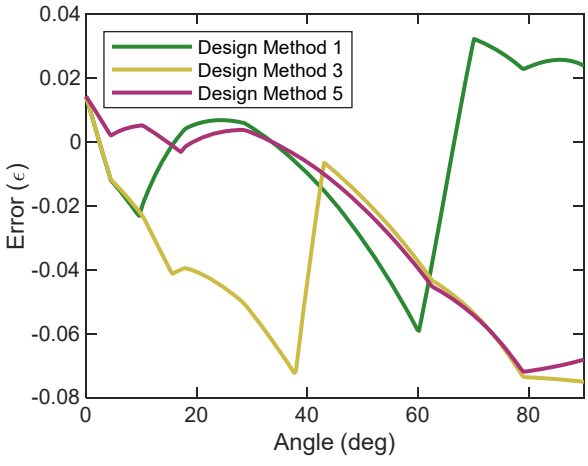

(f) Error measured against second-order inelastic analysis (with residual stress)

Figure 4. Example results for a wide flange subjected to minor-axis bending (Section 1 from Table 1, F_y = 50 ksi) in a sidesway uninhibited frame (Frame 1 from Table 4)

The applied load interaction diagrams from design methods 1, 3, and 5 are compared to that from the second-order inelastic analysis in Figure 4e. These interaction diagrams are largely similar, but not precisely the same. When the applied load interaction diagram for one of the design methods lies outside of the applied load interaction diagram from the second-order inelastic analysis, it implies that the design method permits loads to be applied to the structure that the second-order inelastic analysis has shown result in failure. This represents unconservative error in the design methodology. A radial error measure, ε, defined by Eq. 5 is selected to quantify this error.

$$\varepsilon = \frac{r_{analysis} - r_{design}}{r_{analysis}} \tag{5}$$

where, $r_{analysis}$ is the distance from the origin to the maximum applied loads determined by second-order inelastic analysis and r_{design} is the distance along the same line to the maximum applied loads permitted by the design methodology. Using Eq. 5, unconservative error is represented with negative values.

The error, ε, varies along the interaction diagram, making it necessary to compute its value at many points (i.e., for many angles between the horizontal and vertical axis). The error for design methods 1, 3, and 5 is shown in Figure 4f as a function of the angle from the horizontal axis. The error values for this case range from 7.5% unconservative for design method 3 to 3.2% conservative for design method 1. No firm standard for the maximum permitted unconservative error exists. One reference suggests a maximum of 5% unconservative error (ASCE 1997). Another investigation found unconservative errors of up to 15% (Wang and Ziemian 2019).

6. Results

The most basic result that can be obtained from these analyses is the range of error between the second-order inelastic analyses and the design methods. Table 7 presents the maximum unconservative error (i.e., minimum value of ε) for each section type and each design method listed in Table 6. The values presented are the minimum over the interaction diagrams for each case investigated. 690 wide flange cases, 414 square and rectangular HSS cases, and 207 round HSS cases were investigated. Each of these numbers is the number of steel shapes times three different yield strengths times 23 different frame configurations. Similarly, Table 8 presents the maximum conservative error (i.e., maximum value of ε).

Table 7. Maximum unconservative error (minimum value of ε)

Section Type	Design Method Index (see Table 6)				
	1	2	3	4	5
Wide flange (major-axis bending)	-6.8%	-3.8%	-10.1%	-5.9%	-7.7%
Wide flange (major-axis bending, no RS)	-6.2%	-3.1%	-8.9%	-4.7%	-6.7%
Wide flange (minor-axis bending)	-15.4%	-12.7%	-12.7%	-12.7%	-13.9%
Wide flange (minor-axis bending, no RS)	-13.9%	-10.4%	-10.4%	-10.4%	-13.5%
Square and rectangular HSS	-12.3%	-8.4%	-11.2%	-13.4%	-12.0%
Round HSS	-11.0%	-7.2%	-10.2%	-12.9%	-10.7%

Overall, the methods presented in the AISC *Specification* and investigated here are accurate. Over this broad range of cases, no unconservative error is greater than 15.4% and no

conservative error is greater than 27.6%. The range of errors is significantly greater for steel-concrete composite columns (Denavit et al. 2016).

Table 8. Maximum conservative error (maximum value of ε)

Section Type	Design Method Index (see Table 6)				
	1	2	3	4	5
Wide flange (major-axis bending)	23.8%	22.8%	22.8%	23.5%	19.4%
Wide flange (major-axis bending, no RS)	24.9%	25.6%	25.6%	27.6%	19.7%
Wide flange (minor-axis bending)	21.4%	23.2%	21.3%	22.3%	21.5%
Wide flange (minor-axis bending, no RS)	24.0%	24.8%	23.2%	26.5%	23.1%
Square and rectangular HSS	21.5%	19.8%	19.8%	21.0%	19.1%
Round HSS	20.9%	19.1%	19.1%	20.9%	18.9%

While informative, the overall maximum unconservative and conservative errors do not represent the impact of specific code provisions on individual cases. Such data can be obtained by comparing design methods against each other using a variation of Eq. 5. For example, the impact of the option provided in Section C2.3(c) of the AISC *Specification* to set $\tau_b = 1.0$ can be quantified by comparing design methods 3 and 4 (Table 6). Over the range investigated, invoking this option results in a maximum of 8% increase and a maximum of 8% decrease in maximum permitted applied loads. Similarly, the impact of the option to treat the notional load as a minimum lateral load given in Section C2.2b(d) of the AISC *Specification* can be quantified by comparing design methods 2 and 3. Over the range investigated, invoking this option results in a maximum of 11% increase in maximum permitted applied loads (the option never decreases maximum permitted applied loads).

Figure 5 presents a box plot of the maximum unconservative error broken out by frame configuration. The results presented are for wide flange shapes subjected to minor-axis bending and the design by advanced elastic analysis method compared against second-order inelastic analysis with residual stresses. For each frame configuration, 30 values of the maximum unconservative error were computed, one for each of the cross sections investigated. The red line depicts the median result. The blue box depicts the range from the 25th percentile to the 75th percentile. The black whiskers depict the entire range of the 30 maximum unconservative errors. The results of Figure 5 make clear that the sidesway inhibited cases (frame indices 20-23, Table 4) are the most problematic for the design methodology. The results for other section types showed similar trends for the design by advanced elastic analysis method. For the other design methods, a broader range of frame configurations, including those with high leaning column load, exhibited greater unconservative error.

Figure 6 presents a box plot like Figure 5 but with results broken out by cross section (Table 1). While there is significant overlap in the results, the greatest unconservative errors are seen to occur with the shapes with the greatest shape factor, confirming that this parameter is important to stability behavior and the accuracy of stability design methods.

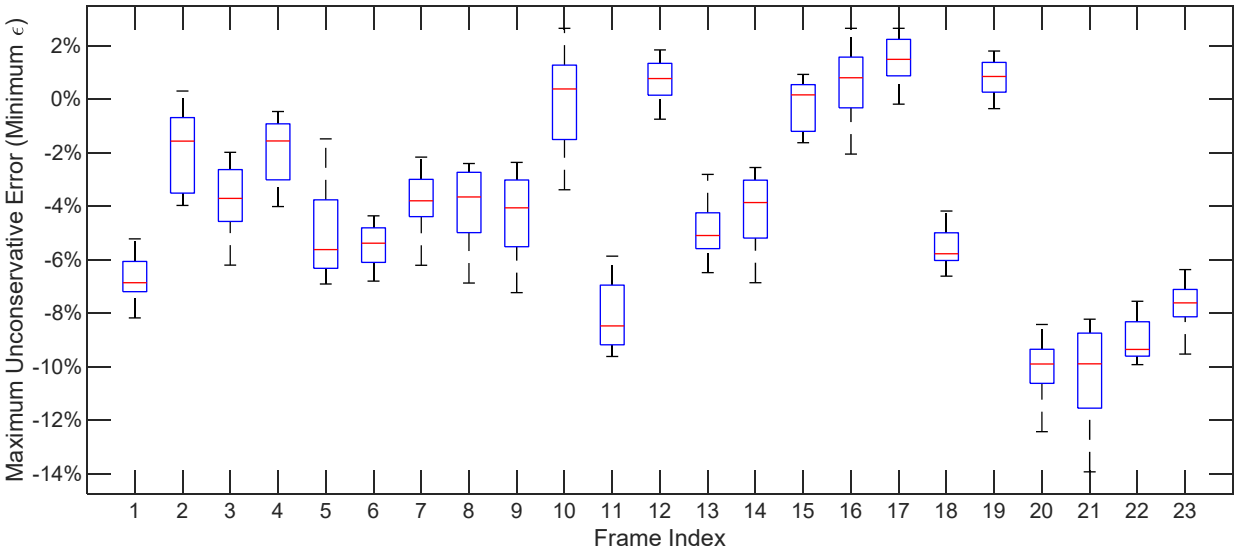

Figure 5. Box plot of maximum unconservative error for each case sorted by frame index – wide flange shapes subjected to minor-axis bending – advanced elastic analysis method compared against second-order inelastic analysis with residual stresses

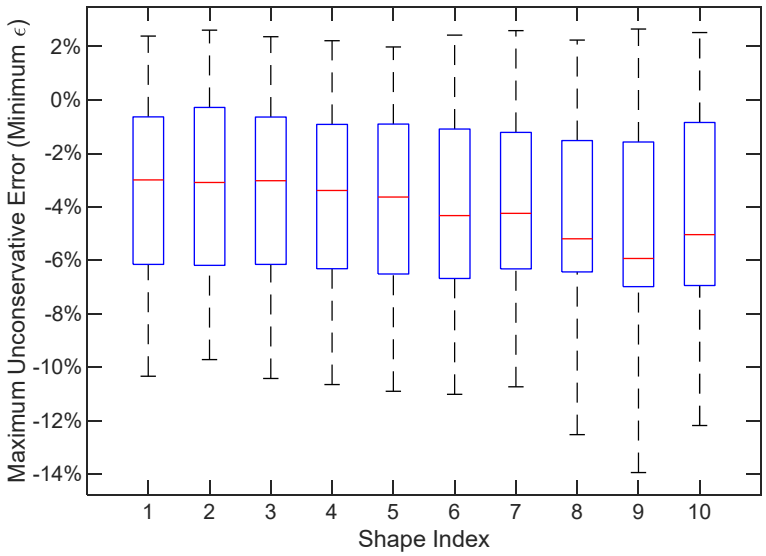

Figure 6. Box plot of maximum unconservative error for each case sorted by section index – wide flange shapes subjected to minor-axis bending – advanced elastic analysis method compared against second-order inelastic analysis with residual stresses

7. Conclusions

This paper presents expanded validation studies for the methods of stability design presented in the AISC *Specification* that are based on second-order elastic analysis. Results from second-order inelastic analyses on a wide range of small structures encompassing different cross section types and geometries, material properties, and frame configurations were used as a benchmark against which the design methods were compared. The following conclusions were made:

- The methods of design presented in the AISC *Specification* are largely accurate.
- Unconservative errors of up to 15% were noted for some cases.

- Error was found to vary with the assumed level of residual stress, however unconservative error remained even if it was assumed that no residual stress was present.
- The unconservative error for the design by advanced inelastic analysis method was found to be most severe for the sidesway inhibited frames.
- The magnitude of unconservative error was found to be correlated with the cross section shape factor.

The results presented in this paper are only a small portion of what is possible with the data generated from the parametric study. It is anticipated that these results will motivate future studies, including further exploration of the data generated in this work, potentially with the goal of refining or expanding options in design methods and investigations using more detailed models that are capable of capturing local buckling and three-dimensional (out-of-plane) behavior.

References

Abdel-Rahman, N., and Sivakumaran, K. S. (1997). "Material Properties Models for Analysis of Cold-Formed Steel Members." *Journal of Structural Engineering*, ASCE, 123(9), 1135–1143.

AISC. (2016). *Specification for Structural Steel Buildings*. American Institute of Steel Construction, Chicago, Illinois.

ASCE. (1997). *Effective Length and Notional Load Approaches for Assessing Frame Stability: Implications for American Steel Design*. American Society of Civil Engineers, Reston, Virginia.

Denavit, M. D., Hajjar, J. F., Perea, T., and Leon, R. T. (2016). "Stability Analysis and Design of Composite Structures." *Journal of Structural Engineering*, ASCE, 142(3), 04015157.

Galambos, T. V., and Ketter, R. L. (1959). "Columns under Combined Bending and Thrust." *Journal of Engineering Mechanics Division*, ASCE, 85(2), 1–30.

Ge, X., and Yura, J. A. (2019). "The strength of rotary-straightened steel columns." *Proceedings of the Annual Stability Conference Structural Stability Research Council*, St. Louis, Missouri.

Kanchanalai, T. (1977). *The Design and Behavior of Beam-Columns in Unbraced Steel Frames*. CESRL Report No. 77-2, Structures Research Laboratory, Department of Civil Engineering, The University of Texas at Austin, Austin, Texas.

Surovek-Maleck, A. E., and White, D. W. (2004). "Alternative Approaches for Elastic Analysis and Design of Steel Frames. II: Verification Studies." *Journal of Structural Engineering*, ASCE, 130(8), 1197–1205.

Wang, Y., and Ziemian, R. D. (2019). "Design by Advanced Elastic Analysis - an investigation of beam-columns resisting minor-axis bending." *Proceedings of the Annual Stability Conference*, Structural Stability Research Council, St. Louis, Missouri.